

# Air-to-Air Communications Beyond 5G: A Novel 3D CoMP Transmission Scheme

Yan Li, Nikolaos I. Miridakis, *Senior Member, IEEE*,

Theodoros A. Tsiftsis, *Senior Member, IEEE*, Guanghua Yang, *Senior Member, IEEE*,  
and Minghua Xia, *Member, IEEE*

## Abstract

In this paper, a novel 3D cellular model consisting of aerial base stations (aBSs) and aerial user equipments (aUEs) is proposed, by integrating the coordinated multi-point (CoMP) transmission technique with the theory of stochastic geometry. For this new 3D architecture, a tractable model for aBSs' deployment based on binomial Delaunay-tetrahedralization is developed, which ensures seamless coverage for a given space. In addition, a versatile and practical frequency allocation scheme is designed to eliminate the inter-cell interference effectively. Based on this model, performance metrics including the ergodic data rate and coverage probability are derived for two types of aUEs: *i*) general aUE (i.e., an aUE having distinct distances from its serving aBSs) and *ii*) the worst-case aUE (i.e., an aUE having equal distances from its serving aBSs). Simulation and numerical results demonstrate that the proposed approach emphatically outperforms the conventional binomial-Voronoi tessellation without CoMP. Insightfully, it provides a similar performance as to the binomial-Voronoi tessellation which utilizes the conventional CoMP scheme; yet, introducing a considerably reduced computational complexity and backhaul/signaling overhead.

## Index Terms

3D cellular model, aerial network, coordinated multi-point (CoMP) transmission, frequency allocation, stochastic geometry, unmanned aerial vehicle (UAV) communications.

Y. Li and M. Xia are with the School of Electronics and Information Technology, Sun Yat-sen University, Guangzhou, 510006, China. M. Xia is also with the Southern Marine Science and Engineering Guangdong Laboratory, Zhuhai 519082, China (e-mail: liyan228@mail2.sysu.edu.cn; xiamingh@mail.sysu.edu.cn).

N. I. Miridakis is with the Institute of Physical Internet, School of Electrical and Information Engineering, Jinan University, Zhuhai, 519070, China. He is also with the Dept. of Informatics and Computer Engineering, University of West Attica, 12243, Greece, and with the Dept. of Informatics, University of Piraeus, 18534, Greece (e-mail: nikozm@uniwa.gr).

T. A. Tsiftsis and G. Yang are with the School of Intelligent Systems Science and Engineering, Jinan University, Zhuhai 519070, China, and also with the Institute of Physical Internet, Jinan University, Zhuhai, 519070, China (e-mail: {theo\_tsiftsis, ghyang}@jnu.edu.cn).

## I. INTRODUCTION

With the ever-increasing number of unmanned aerial vehicles (UAVs), drone-based wireless communications are expected to play a pivotal role to the establishment of the upcoming future networking infrastructures [1], [2]. Due to their inherent mobility and flexibility, they can act as either aerial base stations (aBSs) or aerial user equipments (aUEs). The former nodes can be used to support wireless connectivity for existing terrestrial base stations (BSs) by providing reliable and cost-effective on-the-fly communication. Also, they can offer additional throughput and coverage in some hotspot areas or to assist on emergency or disaster and critical situations. The latter nodes essentially act as mobile terminals or relays under the Internet of Things (IoT) and the emerging Internet-of-Space/Things use cases, by improving the connectivity and coverage of ground devices. They can also play a key role in surveillance and package delivery. Despite such attractive opportunities for UAVs, wireless communications via aerial nodes still face a number of challenges. Regarding aBSs, a key challenge is the three-dimensional (3D) deployment as well as other problems including the resource allocation, trajectory optimization, air-to-ground channel modeling, and performance analysis of aBS-enabled networks. Regarding aUEs, the key challenge is how to get reliable and high-throughput communication, since the existing terrestrial BSs are mainly designed for serving terrestrial UEs, whereas they fail in meeting the high capacity/coverage demands of aUEs. Therefore, using aBSs to serve aUEs is quite promising and presents a requisite for future 5G-and-beyond networking setups [3].

### A. *Related Works and Motivation*

There is a number of works focusing on wireless communications via UAVs. The theoretical investigation considering aUEs can be traced back to [4], where the coverage probability was analyzed therein. Another performance metric, the downlink achievable rate for aUEs served by terrestrial BSs, was considered in [5]. By assuming that the typical aUE is located at a fixed altitude and all the terrestrial BSs are distributed according to a homogeneous Poisson point process (PPP), a tractable coverage probability was derived for aUEs in [6]. Further, by assuming that each aUE is equipped with a tilted directional antenna, an exact downlink coverage probability was derived in [7]. On the contrary, for the scenario where a number of terrestrial UEs are being served by a single (common) aBS, a joint optimization algorithm was designed to maximize the minimum average rate among multiple UEs in [8]. Extending a single aBS to multiple ones, two UAV-based communication scenarios with exact hover time constraints were investigated

and the maximum average data service was reached for terrestrial UEs in [9]. To increase the number of covered terrestrial UEs with minimum transmit power, an optimal placement algorithm regarding aBSs was proposed in [10]. Further, an integral expression for the downlink coverage probability of terrestrial UEs was presented in both [11] and [12], while a tractable expression on the ergodic data rate of terrestrial aUEs was given in [13]. In [14], the coverage probability of a terrestrial UE was analytically studied when it is being served by multiple aBSs, in the case when the latter nodes make transitions in vertical and spatial directions by following a simple mixed mobility model for 3D UAV movement process.

Nevertheless, all the aforementioned works were based on the air-to-ground model; either the case when aBSs provide wireless links for terrestrial UEs, or terrestrial BSs offer connectivity for aUEs. The scenario in which aUEs are being served by aBSs in an entirely aerial networking platform has not studied in the appropriate depth so far. In fact, quite recently, a new 3D cellular architecture for aBSs' deployment based on truncated octahedron shapes was proposed in [15]. However, such a cell structure was extremely complex and no closed-form expressions were attained. Besides, concerning UAV-to-UAV systems, the statistical features of the received signal-to-noise ratio (SNR) were defined in [16], while an efficient iterative algorithm to maximize the net uplink sum-rate was proposed in [17]. To date, both the deployment of 3D aBSs and performance analysis of a fully-fledged aerial communication network, integrating both aBSs and aUEs, is still an open problem.

Further, most of the existing 3D models for aBSs' deployments are based on Poisson-Voronoi tessellation, which is a direct extension of the 2D plane [18]–[21]. However, the performance of cell-edge aUEs in Voronoi models is interference limited, as they have farther distance from the serving aBS and experience stronger inter-cell interference (ICI), as compared to the cell-centric aUEs. Coordinated multi-point (CoMP) transmission is a promising method to improve the aUEs' performance, where a typical aUE selects aBSs on a dynamic basis, according to the received strongest signals. In practice, a typical aUE can choose one, two, or more aBSs to cooperate and work with so as to enhance its total received signal strength and overall communication quality. Nonetheless, this approach is achieved at the cost of producing an overwhelming searching complexity and feedback overhead.

On another front, most of the existing literature works related to UAV-based communications are based on PPP modeling, which is in fact not adequate since only a small number of aBSs are required to cover a given finite space. Moreover, although infinite homogeneous PPP has been widely used to model the

spatial locations of terrestrial BSs or aBSs, the analytical framework of previous works was essentially relied on the condition that the path-loss exponent, say  $\alpha$ , is greater than the space dimension, which is not suitable for line-of-sight (LoS) communication in the considered 3D (aerial) free-space platform, where  $\alpha \leq 3$  usually holds. Particularly, the characteristic functional of a given PPP, say  $\Phi$ , is not applicable if  $\alpha \leq 3$  because the total interference  $I \triangleq \sum_{x \in \Phi} \|x\|^{-\alpha}$  is almost surely (a.s.) non-convergent, where  $\|\cdot\|$  reflects the Euclidean distance. More specifically, by recalling the Campbell's theorem [22, Theorem 4.6], the total interference is absolutely convergent a.s. if and only if the condition  $\int_{\mathbb{R}^3} \min(1, \|x\|^{-\alpha}) dx < \infty$  is satisfied [22, Eq. (4.5)]. To investigate this, by applying Campbell's theorem to the mean of total interference,  $I$ , we have

$$\mathbb{E}(I) = \mathbb{E} \left( \sum_{x \in \Phi} \|x\|^{-\alpha} \right) = \lambda \int_{\mathbb{R}^3} \|x\|^{-\alpha} dx = \begin{cases} \frac{1}{3-\alpha} 4\pi \lambda r^{3-\alpha} \Big|_0^\infty, & \alpha \neq 3 \\ 4\pi \lambda \ln r \Big|_0^\infty, & \alpha = 3 \end{cases}, \quad (1)$$

where  $\mathbb{E}[\cdot]$ ,  $r$ , and  $\lambda$  denote the expectation operator, coverage radius, and the density of  $\Phi$ , respectively. Clearly, if  $\alpha > 3$ ,  $\mathbb{E}(I)$  is finite and the condition [22, Eq. (4.5)] is always satisfied.<sup>1</sup> If  $\alpha \leq 3$ , however, the discussed condition is not satisfied and the interference computed by (1) is infinite.

Unlike PPP, the homogeneous binomial point process (BPP) [22], [23] is more suitable for UAV-based communications. In fact, BPP has received considerable attention in 2D cellular and ad-hoc networks [24]–[26]. However, the outage probability was usually derived by assuming that a typical UE was served by a given transmitter (not a point of BPP) at a fixed distance. Recently, considering the scenario that serving BSs for the typical UE will be chosen from the BPP itself, the exact performance analysis for this network was conducted in [27]. Using the distance distributions derived in [23], [27], [28], the downlink coverage probability of terrestrial UEs based on aBSs networks was firstly analyzed in [11]. Nonetheless, BPP has not been used to model 3D deployments integrating aBSs and aUEs, to the best of our knowledge.

The motivation of this paper is triggered by the recent works [29], [30], where the Poisson-Delaunay triangulation was used to model two-dimensional (2D) cellular networks and a novel CoMP transmission scheme was proposed. This principle is expanded here to model the considered 3D spatial deployment, which is expected to be an indispensable component of future 5G-and-beyond space-air-ground integrated networking setups [31]. The benefits behind the selection of binomial-Delaunay tetrahedralization

<sup>1</sup>The divergence of the mean is caused due to the singularity of the path-loss law, which is a modeling of artifact, since a receiver cannot get more power than the total transmit power of interfering BSs. To address this issue, the path-loss model can be replaced by  $\ell(x) = \min\{1, \|x\|^{-\alpha}\}$  or  $\ell(x) = (1 + \|x\|^{-\alpha})$ . Then, this issue is solved at  $r \rightarrow 0$  and  $\mathbb{E}(I)$  is finite, as long as  $\alpha > 3$  [22, p. 146].

used for the newly proposed 3D joint-transmission CoMP (JT-CoMP) is twofold: *i*) over all possible tetrahedralizations of a 3D point set, the Delaunay tetrahedralization minimizes the maximum enclosing radius of any simplex, where the enclosing radius of a simplex is defined as the minimum radius of an enclosing sphere [32]; and *ii*) the cooperation set for an aUE is *fixed and uniquely* determined by the geometric locations of its nearby aBSs. In this study, BPP is used to simulate the aBSs' locations and Delaunay tessellation is used for 3D cellular network modeling. The resulting network model is called binomial-Delaunay tetrahedralization. This is in contrast to the conventional CoMP in binomial-Voronoi cells, where the said cooperation should be dynamically defined; thereby, causing extensive signaling overhead. Besides, assuming  $N$  aBSs and compared to the typical dynamic cooperation in a 3D binomial-Voronoi network, which provides an average (normalized) volume  $1/N$  [33, Table 5.5.2], the proposed scheme introduces a corresponding average volume  $35/(24\pi^2 N) \approx 1/(7N)$  [33, Table 5.11.2]. This implies approximately a 7-fold total improvement of the network coverage probability and spectral efficiency.

## B. Contributions

The main contributions of this paper are summarized as follows.

- 1) Network model: We propose a novel 3D cellular model based on binomial-Delaunay tetrahedralization. More specifically, 3D CoMP transmission is applied (as an extension of the typical 2D CoMP case in planar terrestrials) in order to further boost the overall communication quality. Particularly, a joint-transmission CoMP (JT-CoMP) scheme is proposed, where each aUE is being simultaneously served by four aBSs using the same system resources, thus forming tetrahedral cells.
- 2) Performance analysis: Both the average data rate and coverage probability expressions are derived for the general aUE (i.e., the typical aUE having distinct distances from its serving four aBSs). Corresponding expressions are also provided for the worst-case aUE (i.e., when the typical aUE is located at an equidistant point with regards to its four serving aBSs).
- 3) Frequency planning: A practical frequency allocation is developed so as to effectively mitigate ICI. Based on this strategy, each networking cell operates in different frequency bands according to a fast greedy coloring algorithm. Actually, a practical frequency allocation is proposed, where the most efficient space filling mode, called *face-centered cubic* (FCC) packing [34, Section 6.3], is adopted to fill the entire 3D space. The entire process is indeed a graph coloring problem, where each tetrahedral

cell denotes a graph node and the goal is to allocate different colors (i.e., spectrum resources) to each cell appropriately.

### C. Organization of the Paper

The rest of this paper is organized as follows. Section II describes the system model and the types of aUEs. Then, Sections III is devoted to the performance analysis of both general aUE and worst-case aUE, where the corresponding ergodic data rate and coverage probability of the typical aUE are explicitly derived. Next, a frequency planning scheme is developed in Section IV. Simulation and numerical results are discussed in Section V and, finally, Section VI concludes the paper.

## II. SYSTEM MODEL

As illustrated in Fig. 1, we consider a 3D wireless communication system consisting of UAVs or drones. In particular, let a certain type of drones be aBSs, which serve another type of drone aUEs in the downlink. Further, aBSs are interconnected with the core network via high-altitude platforms (HAPs) and/or terrestrial BSs, while aUEs forward data to their associated terrestrial UEs. Each aBS supports a full 3D connectivity to its corresponding aUEs. Moreover, we consider a BPP network  $\Phi$ , with  $N$  transmitting aBSs uniformly distributed in a finite ball  $b(0, R)$  centered at the origin  $o = (0, 0, 0)$  with radius  $R$ . By using the criteria of the nearest neighbor association, namely, each aUE is directly connected with its nearest aBS, 3D binomial-Voronoi cells are therefore being formed. Unfortunately, the typical cell of this Voronoi tessellation is too complex to be mathematically tractable even in 2D space [35]. It is noteworthy at this point to state that for an arbitrary dimensional binomial-Voronoi tessellation, its dual-graph is the so-called binomial-Delaunay triangulation as shown in Fig. 2. In the 3D case of interest considered herein, it is known as binomial-Delaunay tetrahedralization.

By recalling the Slivnyak-Mecke theorem in the theory of stochastic geometry [36, p. 132], a typical aUE can be assumed to be located at the origin  $(0, 0, 0) \in \mathbb{R}^3$ , without loss of generality. By using the propagation model with path-loss exponent being  $\alpha$ , we can express the instantaneous received signal-to-interference-plus-noise ratio (SINR) at the typical aUE as

$$\Gamma = \frac{\left| \sum_{i \in \mathcal{C}_0} \kappa_i^{\frac{1}{2}} P_i^{\frac{1}{2}} d_i^{-\frac{\alpha}{2}} \right|^2}{\sum_{\Phi \setminus \mathcal{C}_0} \kappa_k P_k d_{k,0}^{-\alpha} + \sigma_0^2}, \quad (2)$$

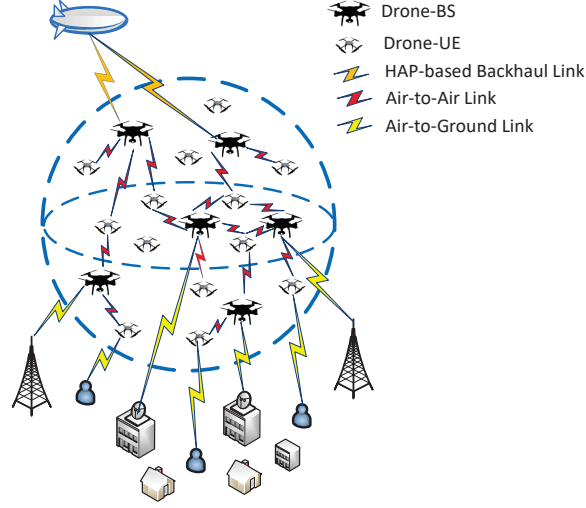


Fig. 1. Conceptual model of 3D wireless communication systems.

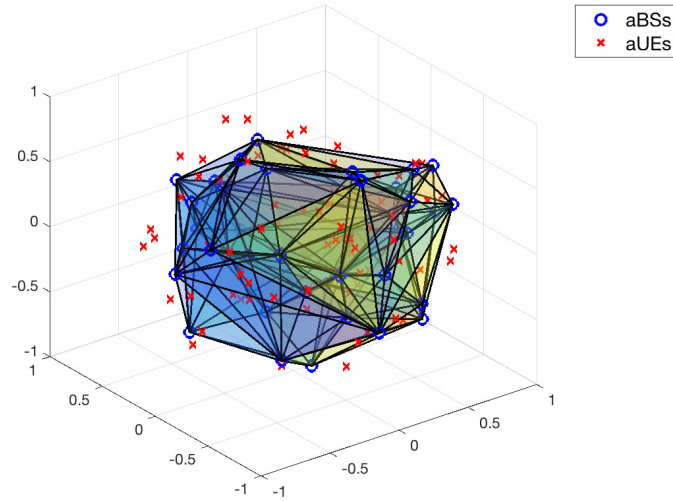


Fig. 2. An illustrative cellular network modeled by the Poisson-Delaunay tetrahedron, where the blue-circles refer to the drone aBSs and the cross-marks denote the drone aUEs with a normalized coverage volume of one cubic kilometers.

where the numerator denotes the power of desired signals originating from the cooperating set  $\mathcal{C}_0 = \{A_0, B_0, C_0, D_0\}$ . The first term in the denominator represents the power of inter-cell interfering signals coming from the remaining aBSs in the set  $\Phi \setminus \mathcal{C}_0$ . Specifically,  $\kappa_i$  stands for a fixed (known) system parameter incorporating antenna gains and (reference) propagation attenuation of the considered path loss model.  $P_i$  denotes the transmit power of the  $i^{\text{th}}$  aBS;  $d_i$  indicates the distance between the  $i^{\text{th}}$  aBS and the typical aUE, and  $\sigma_0^2$  refers to the noise power. Finally, notice that the intra-cell interference is not accounted for in (2) since it can be readily mitigated by classical time and/or frequency division

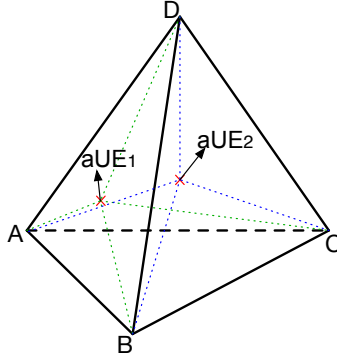


Fig. 3. Two types of aUEs: aUE<sub>1</sub> has distinct distances to its four serving aBSs  $\{A, B, C, D\}$  whereas aUE<sub>2</sub> has identical distance to them.

multiplexing techniques.

Since only a single-tier cellular network and the downlink transmission without power control are considered, the transmit powers of all aBSs are assumed identical and normalized to be unity. Moreover, the fixed system parameters between aBSs and aUEs are assumed identical, that is,  $\kappa_i = \kappa_k \triangleq \kappa$ , for all  $i \in \mathcal{C}_0$  and  $k \in \Phi \setminus \mathcal{C}_0$ . Meanwhile, as the network performance under study is typically interference-limited, the noise term in (2), i.e.,  $\sigma_0^2$ , is negligible. Accordingly, by canceling out the constant term  $\kappa P$  in (2), the signal-to-interference ratio (SIR) stems as

$$\Gamma_1 = \frac{\left| \sum_{i \in \mathcal{C}_0} d_i^{-\frac{\alpha}{2}} \right|^2}{\sum_{k \in \Phi \setminus \mathcal{C}_0} d_{k,0}^{-\alpha}}. \quad (3)$$

As illustrated in Fig. 3, we consider two types of aUEs based on their locations in a given tetrahedral cell; namely, *i*) general aUE referring to an aUE having distinct distances to its four serving aBSs (e.g., aUE<sub>1</sub> in Fig. 3); and *ii*) the worst-case aUE which is located at the centroid of the cell, being equidistant from its four serving aBSs (e.g., aUE<sub>2</sub> in Fig. 3).

To measure the effectiveness of CoMP operation based on the binomial-Delaunay tetrahedralization, we investigate two performance metrics, namely, the ergodic data rate and coverage probability. In fact, the ergodic data rate experienced by a typical aUE is given by [15]

$$\mathcal{R} \triangleq \mathbb{E} [\ln(1 + \Gamma)]. \quad (4)$$

Furthermore, given an outage threshold on the received SIR at a typical aUE, say  $\gamma$ , the coverage probability is defined as [19]

$$\mathcal{P} \triangleq 1 - \Pr \{ \Gamma \leq \gamma \}. \quad (5)$$



### III. PERFORMANCE ANALYSIS

In this section, joint transmission (JT) is applied at the four aBSs within a tetrahedral cooperation set pertaining to both general aUE and the worst-case aUE, whereas the ergodic data rate and coverage probability are used to evaluate their performance.

#### A. General aUE

According to (3), the SIR for the general aUE is explicitly given by

$$\Gamma_1 = \frac{\left| \sum_{i=1}^4 d_i^{-\frac{\alpha}{2}} \right|^2}{\sum_{k=5}^N d_{k,0}^{-\alpha}} = \frac{S_1}{I_1}, \quad (6)$$

where  $S_1 \triangleq \left| \sum_{i=1}^4 d_i^{-\frac{\alpha}{2}} \right|^2$  and  $I_1 \triangleq \sum_{k=5}^N d_{k,0}^{-\alpha}$ . To calculate (4) and (5), we subsequently address the related distance distribution involved in (6). Defining the distance between the  $i^{\text{th}}$  aBS and the typical aUE at the origin as  $D_i$ , the cumulative distribution function (CDF) of  $D_i$  is given by [23]

$$F_{D_i}(r_i) = \left( \frac{r_i}{R} \right)^3, \quad 0 \leq r_i \leq R, \quad (7)$$

and, consequently, the probability density function (PDF) of  $D_i$  can be readily computed as

$$f_{D_i}(r_i) = \frac{3r_i^2}{R^3}. \quad (8)$$

Conditioned on the serving distance  $r$ , the set of distances between the typical aUE and the interfering aBSs  $\{D_i\}_{i=5}^N$ , are independent and identically distributed (i.i.d.) having the following PDF (for more details, please refer to Appendix A)

$$f_{D_i|r}(r_i) = \frac{3r_i^2}{R^3 - r^3}, \quad r \leq r_i \leq R. \quad (9)$$

Based on the theory of order statistics [37, Eq. (2.2.2)], the joint PDF of the nearest four distances is given by

$$f_{d_1, d_2, d_3, d_4}(r_1, r_2, r_3, r_4) = \frac{N!}{(N-4)!} (1 - F_{D_4}(r_4))^{N-4} \prod_{i=1}^4 f_{D_i}(r_i). \quad (10)$$

Substituting (7) and (8) into (10) yields

$$f_{d_1, d_2, d_3, d_4}(r_1, r_2, r_3, r_4) = \frac{N!}{(N-4)!} \left( 1 - \left( \frac{r_4}{R} \right)^3 \right)^{N-4} \prod_{i=1}^4 \frac{3r_i^2}{R^3}. \quad (11)$$

1) *Ergodic Data Rate*: Now, we are in a position to formalize the ergodic data rate of a typical UE in the following theorem.

**Theorem 1.** *The ergodic data rate of a general aUE can be calculated as*

$$\mathcal{R}_1(\alpha) = \int_{\mathbf{r}>0} \int_{z>0} \frac{1}{z} (1 - M_{S_1}) M_{I_1} f_{d_1, d_2, d_3, d_4}(r_1, r_2, r_3, r_4) dz d\mathbf{r}, \quad (12)$$

where  $\mathbf{r} = (r_1, r_2, r_3, r_4)$  with  $r_1 < r_2 < r_3 < r_4$ , and the moment generating functions of  $S_I$  and  $I$  are given by

$$M_{S_1}(z) = \exp \left( -z \left| \sum_{i \in \mathcal{C}_0} d_i^{-\frac{\alpha}{2}} \right|^2 \right) \quad (13)$$

and

$$M_{I_1}(z) = \left( \frac{1}{R^3 - d_4^3} \left( R^3 {}_1F_1 \left[ \begin{matrix} -\frac{3}{\alpha} \\ 1 - \frac{3}{\alpha} \end{matrix}; -zR^{-\alpha} \right] - d_4^3 {}_1F_1 \left[ \begin{matrix} -\frac{3}{\alpha} \\ 1 - \frac{3}{\alpha} \end{matrix}; -zd_4^{-\alpha} \right] \right) \right)^{N-4}, \quad (14)$$

respectively, with  ${}_1F_1[*; *]$  denoting the Kummer's confluent hypergeometric function [38, Eq. 9.210.1].

*Proof:* Using the equality involved in the lemma of [39], which reads

$$\ln \left( 1 + \frac{X}{Y} \right) = \int_{z>0} \frac{1}{z} (1 - \exp(-zX)) \exp(-zY) dz, \quad (15)$$

the ergodic data rate can be derived as

$$\mathcal{R}_1(\alpha) = \int_{\mathbf{r}>0} \mathbb{E} \left[ \ln \left( 1 + \frac{S_1}{I_1} \right) \middle| \mathbf{r} \right] f_{d_1, d_2, d_3, d_4}(r_1, r_2, r_3, r_4) d\mathbf{r} \quad (16)$$

$$= \int_{\mathbf{r}>0} f_{d_1, d_2, d_3, d_4}(r_1, r_2, r_3, r_4) \int_{z>0} \frac{1}{z} \left( 1 - \underbrace{\mathbb{E}[\exp(-zS_1)]}_{M_{S_1}} \right) \underbrace{\mathbb{E}[\exp(-zI_1)]}_{M_{I_1}} dz d\mathbf{r}, \quad (17)$$

where  $\mathbb{E} \left[ \ln \left( 1 + \frac{S_1}{I_1} \right) \middle| \mathbf{r} \right]$  is the conditional ergodic data rate according to (4),  $M_{S_1}(z)$  is previously given by (13) and  $M_{I_1}(z)$  is derived as follows.

$$\begin{aligned} M_{I_1}(z) &= \mathbb{E}_{d_{k,0}} \left[ \exp \left( -z \sum_{k=5}^N d_{k,0}^{-\alpha} \right) \right] = \mathbb{E}_{d_k} \left[ \prod_{k=5}^N \exp(-zd_k^{-\alpha}) \right] \\ &= \left( \mathbb{E}_{d_k} [\exp(-zd_k^{-\alpha})] \right)^{N-4} = \left( \int_{d_4}^R f_{D_i|d_4}(x) \exp(-zx^{-\alpha}) dx \right)^{N-4}. \end{aligned} \quad (18)$$

Substituting (9) into (18) and using [38, Eq. 8.351.2], while performing some straightforward manipulations, we arrive at (14). Inserting (13) and (14) into (17) yields the desired (12). ■

2) *Coverage Probability*: In this subsection, an accurate approximation on the coverage probability for the general aUE is provided. By recalling the causal form of the central limit theorem [40, p. 234], it is

known that the sum of multiple positive i.i.d. variables can be approximated by a Gamma distribution. In particular, for the PDF of  $I_1$ , we have the following lemma.

**Lemma 1.** *The PDF of  $I_1 \triangleq \sum_{k=5}^N d_{k,0}^{-\alpha}$  can be well approximated by the Gamma distribution*

$$f_{I_1}(x) \approx \frac{x^{v(d)-1}}{\Gamma[v(d)]\theta(d)^{v(d)}} \exp\left(-\frac{x}{\theta(d)}\right), \quad (19)$$

where

$$v(d) = \begin{cases} (N-4) \left( \frac{(3-\alpha)^2}{3(3-2\alpha)} (R^3 - d^3)(R^{3-2\alpha} - d^{3-2\alpha})^{-1} - 1 \right)^{-1}, & \alpha \neq 3, \\ (N-4) \left( \frac{1}{9} (d^{-3} - R^{-3})(R^3 - d^3)(\ln R - \ln d)^{-1} - 1 \right)^{-1}, & \alpha = 3, \end{cases} \quad (20)$$

$$\theta(d) = \begin{cases} \frac{3-\alpha}{3-2\alpha} - \frac{3}{(3-\alpha)} (R^3 - d^3)^{-1} (R^{3-2\alpha} - d^{3-2\alpha}), & \alpha \neq 3, \\ \frac{1}{3} (\ln R - \ln d)^{-1} (d^{-3} - R^{-3}) - 3(R^3 - d^3)^{-1} (\ln R - \ln d), & \alpha = 3, \end{cases} \quad (21)$$

and  $\Gamma[\cdot]$  is the Gamma function [38, Eq. (8.310.1)].

*Proof:* See Appendix B. ■

With the aid of Lemma 1, we can derive an accurate approximation for the coverage probability, as the following theorem suggests.

**Theorem 2.** *Given a prescribed outage threshold  $\gamma$ , the coverage probability of a general aUE can be approximated by*

$$\mathcal{P}_1(\gamma, \alpha) \approx \frac{1}{\Gamma[v(d_4)]} \int_{\mathbf{r}>0} \gamma \left( v(d_4), \frac{1}{\gamma \theta(d_4)} \left| \sum_{i=1}^4 d_i^{-\frac{\alpha}{2}} \right|^2 \right) f_{d_1, d_2, d_3, d_4}(r_1, r_2, r_3, r_4) d\mathbf{r}, \quad (22)$$

where  $\gamma(\cdot, \cdot)$  is the lower incomplete Gamma function [38, Eq. (8.350.1)],  $f_{d_1, d_2, d_3, d_4}(r_1, r_2, r_3, r_4)$  is given in (11), and  $v(d_4)$  and  $\theta(d_4)$  are shown in (20) and (21), respectively.

*Proof:* The coverage probability reads as

$$\mathcal{P}_1(\gamma, \alpha) = \int_{\mathbf{r}>0} \Pr(\Gamma_1 > \gamma | \mathbf{r}) f_{d_1, d_2, d_3, d_4}(r_1, r_2, r_3, r_4) d\mathbf{r}, \quad (23)$$

where the probability term in the integrand becomes

$$\Pr(\Gamma_1 > \gamma | \mathbf{r}) = \Pr \left( I_1 < \frac{1}{\gamma} \left| \sum_{i=1}^4 d_i^{-\frac{\alpha}{2}} \right|^2 \right) \quad (24)$$

$$\approx \frac{1}{\Gamma[v(d_4)]} \gamma \left( v(d_4), \frac{1}{\gamma \theta(d_4)} \left| \sum_{i=1}^4 d_i^{-\frac{\alpha}{2}} \right|^2 \right). \quad (25)$$

As earlier stated,  $I_1$  is the sum of multiple conditional i.i.d. random variables. Therefore, by applying

Lemma 1, (24) can be explicitly computed as (25) via [38, Eq. (3.381.1)]. Substituting (25) and the joint distance distribution (11) into (23) yields the intended (22). ■

### B. Worst-Case aUE

In this subsection, the ergodic data rate and coverage probability are analyzed for the worst-case aUE. By recalling Fig. 3, an aUE at the vertex of a tetrahedral cell, e.g., a UE<sub>2</sub>, is chosen as a typical point and set to be the origin in 3D space, which implies that the Euclidean distances between a typical aUE and its serving aBSs are identical, i.e.,  $d_i = d$ , for all  $i \in \mathcal{C}_0$ . Thereby, (3) reduces to

$$\Gamma_2 = \frac{16d^{-\alpha}}{\sum_{k=5}^N d_{k,0}^{-\alpha}}. \quad (26)$$

Also, it holds that the PDF of the equidistant  $d$  follows (the proof is given in Appendix C)

$$f_d(x) = \frac{3}{R} \frac{1}{\beta(N-3,3)} \left(\frac{x}{R}\right)^8 \left(1 - \left(\frac{x}{R}\right)^3\right)^{N-4}. \quad (27)$$

1) *Ergodic Data Rate*: Based on (15) and (27), the ergodic data rate of the worst-case aUE is formalized in the following theorem.

**Theorem 3.** *The ergodic data rate of the worst-case aUE can be computed as*

$$\mathcal{R}_2(\alpha) = \int_{0 < x < R} \int_{z > 0} \frac{1}{z} (1 - M_{S_2}) M_{I_2} f_d(x) dz dx, \quad (28)$$

where

$$M_{S_2}(z) = \exp(-16zd^{-\alpha}), \quad (29)$$

$$M_{I_2}(z) = \left( \frac{1}{R^3 - d^3} \left( R^3 {}_1F_1 \left[ \begin{matrix} -\frac{3}{\alpha} \\ 1 - \frac{3}{\alpha} \end{matrix}; -zR^{-\alpha} \right] - d^3 {}_1F_1 \left[ \begin{matrix} -\frac{3}{\alpha} \\ 1 - \frac{3}{\alpha} \end{matrix}; -zd^{-\alpha} \right] \right) \right)^{N-4}. \quad (30)$$

*Proof*: The proof is similar to that of Theorem 1 and, thus, it is omitted for brevity. ■

2) *Coverage Probability*: Using the same method as in Theorem 2, the coverage probability for the worst-case aUE can be derived, as summarized in the following theorem.

**Theorem 4.** *The coverage probability of the worst-case aUE is approximated by*

$$\mathcal{P}_2(\gamma, \alpha) \approx \frac{1}{\Gamma[v(d)]} \int_{d > 0} \gamma \left( v(d), \frac{16d^{-\alpha}}{\gamma \theta(d)} \right) f_d(x) dx, \quad (31)$$

where  $f_d(x)$  is given by (27), and  $v(d)$  and  $\theta(d)$  are shown in (20) and (21), respectively.

#### IV. FREQUENCY PLANNING AND INTERFERENCE MITIGATION

This section develops a practical frequency planning strategy so as to sufficiently reduce ICI. In particular, the frequency division multiple access (FDMA) scheme is adopted herein.<sup>2</sup> Doing so, each four-node aBS set forming a tetrahedral cell occupies a unique frequency band for its underlying aUEs. Nonetheless, a given aBS could be interconnected simultaneously to multiple tetrahedra, reflecting that each aBS should be able to reserve a corresponding number of available (i.e., non-overlapping, non-occupied) frequency bands. Therefore, the proposed drone-based wireless cellular network can be visualized as a 3D colored graph, consisting of multiple non-overlapping tetrahedra. Each tetrahedron has a unique color reflecting the corresponding frequency band to serve its associated aUEs. Also, the number of distinct frequency bands that a given aBS must preserve is determined by its corresponding graph degree and the number of aUEs inside that every tetrahedron is linked with. For a sufficient spectrum resource, whenever the number of aBSs is relatively low (e.g.,  $N < 20$ ), the said condition may be feasible. However, as the number of aBSs increases, the corresponding spectrum resources per each cell become quite narrow. To this end, a frequency reuse scheme is required in accordance to the typical 2D cellular infrastructures.

##### A. Face-Centered Cubic Packing

As illustrated in Fig. 4, the *face-centered cubic* (FCC) packing is widely adopted to fill the entire 3D space [34, Section 6.3]. In particular, Fig. 4a shows the close-packing of equal spheres of radius  $r$ , which is in geometry a dense arrangement of congruent spheres in an infinite, regular manner (i.e., lattice). Figure 4b illustrates FCC packing in a cubic of edge length  $a$ , where the spheres are situated at the corners of the cubic and at the centers of all the cube faces. To guarantee a close-packed arrangement, namely, there is no way to pack more spheres into the cubic, we must have  $a = 2\sqrt{2}r$  and, hence, the packing efficiency is  $\delta = \mathcal{V}_{\text{Sphere}}/\mathcal{V}_{\text{Cube}} = (16\pi r^3/3)/(16\sqrt{2}r^3) \simeq 74\%$ . As proved in [41], this is the highest packing efficiency achieved by a lattice packing.

Now, we integrate the methodology of FCC packing into our binomial Delaunay-tetrahedralization for frequency planning. The main idea is to use each sphere in Fig. 4a to represent a cluster of tetrahedra. The same spectrum resource is reused among spheres whereas in each sphere, the spectrum resource is orthogonally allocated to different tetrahedra. As a result, the frequency allocation strategy is a solution to

<sup>2</sup>Other orthogonal multiple access schemes can alternatively be used instead, such as time division multiple access (TDMA) or orthogonal FDMA (OFDMA), without affecting the main results presented hereinafter.

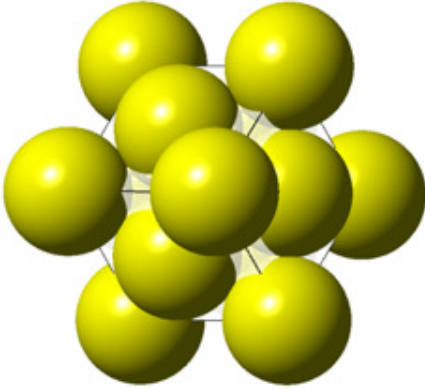
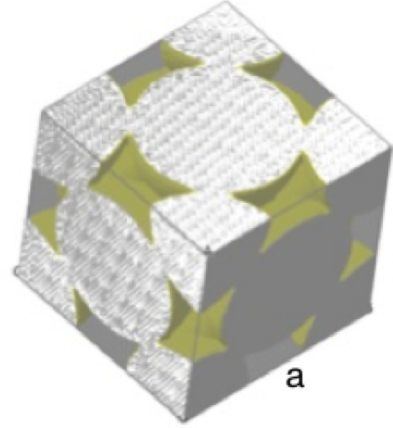
(a) Close-packing of equal spheres of radius  $r$ .(b) FCC packing in a cubic of edge length  $a$ .

Fig. 4. The principle of face-centered cubic (FCC) packing.

the well-known graph coloring problem, where each tetrahedron denotes a graph node and the goal is to allocate different colors (i.e., frequency bands) to each tetrahedron lying within its corresponding sphere.

Prior to further proceeding, as shown in Fig. 5, we define three types of tetrahedral cells: *i) Standard cell*: It refers to a tetrahedron whose vertices (thus, its whole volume) are located inside a given sphere; *ii) Residual cell*: It stands for a tetrahedron whose volume does not entirely belong to a particular sphere. It may be ‘spatially connected’ to more than one sphere; and *iii) Independent cell*: It indicates a tetrahedron whose volume falls entirely outside any given sphere, i.e., in the gap between tangent spheres. For illustration purposes, Fig. 6 depicts two filling spheres (one is blue and the other is yellow), and the red circles refer to aBSs involved in the two spheres whereas the blue circles refer to the remaining aBSs. The tetrahedra with red boundaries illustrates the three types of cells involved in the two spheres.

### B. Frequency Reuse Distance

To further elaborate on the frequency reuse criterion, the *effective interference radius*,  $\epsilon$ , is defined such that each interfering aBS using the same frequency band should be outside this region. The ergodic data rate is selected as a standard performance metric. In particular, the following condition should be satisfied:

$$\mathbb{E} [\ln(1 + \Gamma)] \geq \mathcal{R}_{\text{th}}, \quad (32)$$

where  $\mathcal{R}_{\text{th}}$  stands for a predetermined minimum data rate of every aUE in the network under study (in nat/sec/Hz). Since we consider a fully-fledged aerial wireless cellular system consisting entirely of drones,

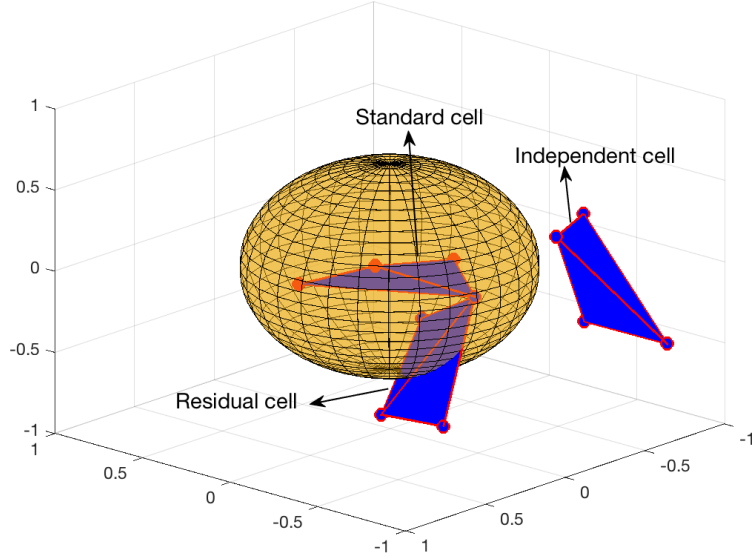


Fig. 5. Three types of tetrahedral cells with respect to a reference sphere, where ‘o’ denotes the drone aBSs.

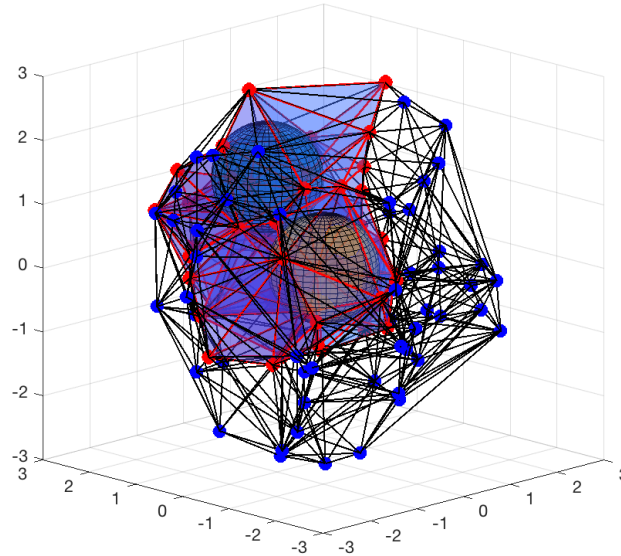


Fig. 6. An illustrative example of CoMP transmission based on binomial-Delaunay tetrahedralization with two filling spheres, where red circles denote the drone aBSs involved in the two observed spheres and the blue circles refer to the remaining aBSs.

the path loss exponent is set to  $\alpha = 2$ . Also, let  $b(o, \epsilon)$  be a sphere with radius  $\epsilon$  centered at the origin  $o$ ,

$X \triangleq |\sum_{i \in \mathcal{C}_0} d_i^{-1}|^2$ , and  $Y_\epsilon \triangleq \sum_{k \in \Phi \setminus b(o, \epsilon)} d_{k,0}^{-2}$ . It is straightforward that

$$\mathbb{E} \left[ \ln \left( 1 + \frac{X}{Y_\epsilon} \right) \right] \leq \ln \left( 1 + \mathbb{E} \left[ \frac{X}{Y_\epsilon} \right] \right) \approx \ln \left( 1 + \frac{\mathbb{E}[X]}{\mathbb{E}[Y_\epsilon]} \right), \quad (33)$$

which implies that a large  $\epsilon$  is desired from the received SIR viewpoint as  $\mathbb{E}[Y_\epsilon]$  decreases with  $\epsilon$ . In contrast, as the said sphere  $b(o, \epsilon)$  gets larger, there are more tetrahedral cells in a cluster and each cell gets less spectrum resources. To resolve this dilemma, the optimal spherical radius,  $\epsilon^*$ , is determined by allowing the maximum interference, that is, the inequality (32) takes equality:

$$\ln \left( 1 + \frac{\mathbb{E}[X]}{\mathbb{E}[Y_{\epsilon^*}]} \right) = \mathcal{R}_{\text{th}}, \quad (34)$$

where  $\mathbb{E}[Y_{\epsilon^*}]$  can be computed as

$$\mathbb{E}[Y_{\epsilon^*}] = N \frac{\epsilon^{*3}}{R^3} \int_{\epsilon^*}^R x^{-2} \frac{3x^2}{R^3 - \epsilon^{*3}} dx = \frac{3N\epsilon^{*3}}{R^3 (R^2 + R\epsilon^* + \epsilon^{*2})}, \quad (35)$$

and  $\mathbb{E}[X]$  is evaluated by

$$\mathbb{E}[X] = \int_{\mathbf{r}>0} (r_1^{-1} + r_2^{-1} + r_3^{-1} + r_4^{-1})^2 f_{d_1, d_2, d_3, d_4}(r_1, r_2, r_3, r_4) d\mathbf{r} \quad (36)$$

$$= \frac{65\Gamma(N+1)\Gamma(\frac{10}{3})}{12\epsilon^2\Gamma(N+\frac{1}{3})}, \quad (37)$$

with  $\{\mathbf{r} : 0 < r_1 \leq r_2 \leq r_3 \leq r_4 \leq \epsilon\}$ . As for the worst-case aUE, we have

$$\mathbb{E}[X] = 16 \int_0^\epsilon r^{-2} f_d(r) dr = \frac{8\Gamma(\frac{7}{3})\Gamma(N)}{\epsilon^2\Gamma(N-\frac{2}{3})}, \quad (38)$$

where  $f_d(\cdot)$  was defined earlier in (27).

Next, inserting (37) (or (38)) and (35) into (34) for the general or the worst-case aUEs, respectively, the numerical results for the optimal spherical radius  $\epsilon^*$  can be computed as per

$$\left( e^{\mathcal{R}_{\text{th}}} - 1 \right) \epsilon^{*5} - \Delta(N)R^3\epsilon^{*2} - \Delta(N)R^4\epsilon^* - \Delta(N)R^5 = 0, \quad (39)$$

with  $\Delta(N) \triangleq \frac{65\Gamma(N+1)\Gamma(\frac{10}{3})}{36N\Gamma(N+\frac{1}{3})}$  for the general aUE, whereas  $\Delta(N) \triangleq \frac{8\Gamma(N)\Gamma(\frac{7}{3})}{3N\Gamma(N-\frac{2}{3})}$  for the worst-case aUE.

The solution  $\epsilon^*$  for the worst-case aUE provides an upper bound for that of the general aUE.

Based on the definition of the sphere  $b(o, \epsilon^*)$ , a cluster of manifold tetrahedral cells is being formed lying within this sphere. Each cell in a given cluster uses distinct spectrum resources so as to eliminate intra-cluster interference. Outside  $b(o, \epsilon^*)$ , the same spectrum resources are reused by other cells forming another cluster, and the entire process is quite similar to the classical planar case. Therefore, frequency reuse factor can be defined as

$$\eta \triangleq \left\lceil \frac{\mathcal{V}_{b(o, \epsilon^*)}}{\mathbb{E}[\mathcal{V}_{\text{cell}}]} \right\rceil, \quad (40)$$



where the numerator and denominator represents the volume of the effective interfering sphere and the expected volume of the typical/reference cell, respectively, and  $\lceil \cdot \rceil$  stands for the ceiling operator. The volume of the sphere  $b(o, \epsilon^*)$  is simply  $\mathcal{V}_{b(o, \epsilon^*)} = 4\pi(\epsilon^*)^3/3$ . Further, according to [33, Table 5.11.2] and [22, Thm. 2.9 and Def. 2.12], we get  $\mathbb{E}[\mathcal{V}_{\text{cell}}] = 35R^3/(18\pi N)$ . As a result, the integer-valued frequency reuse factor is computed by

$$\eta \triangleq \left\lceil \frac{24}{35} N \pi^2 \left( \frac{\epsilon^*}{R} \right)^3 \right\rceil. \quad (41)$$

### C. Frequency Allocation

The basic idea of the proposed frequency allocation strategy is as follows. Given a spherical space of radius  $R$ , there are  $N$  aBSs with each predetermined data rate threshold  $\mathcal{R}_{\text{th}}$ . We first construct the Delaunay tetrahedralization and define the corresponding tetrahedral cells by using, e.g., the radial sweep algorithm or divide-and-conquer algorithm [42, ch. 4]. Then, we compute the radius of sphere  $\epsilon^*$  as per (39), and fill the target space with spheres of radius  $\epsilon^*$  by using FCC packing. For each sphere, count its standard cells and residual cells and, then, sort the resultant spheres in a descending order by starting with the one with the largest number of tetrahedral cells, which is labeled Sphere-1. Given that there are  $k_1$  cells in Sphere-1, the bandwidth reserved for each cell is simply  $\mathcal{B}/k_1$ , where  $\mathcal{B}$  denotes the total bandwidth for the whole system. Finally, apply a fast greedy coloring algorithm [43] with repeated random sequences to assign different spectrum resources for each cell, starting with Sphere-1. This colored pattern is repeated in every sphere such that unique colors are being assigned to cells of the same sphere, meanwhile, the effective interference radius  $\epsilon^*$  is always satisfied for each cell. Finally, all independent cells are identified and randomly assigned colors chosen from Sphere-1.

In summary, the proposed frequency allocation based on greedy coloring is formalized in Algorithm 1. For illustration purposes, Fig. 7 shows five spheres and five tetrahedral cells of the same frequency band, filled in yellow.

**Remark 1** (The maximum number of colors). *In general, the optimal approach for frequency planning is to adopt a greedy coloring algorithm. However, greedy coloring is a well-known NP-hard problem. For practical applications, a heuristic solution is adopted in this paper. Obviously, Algorithm 1 is suboptimal yet practical. The reason is that the color allocation of the underlying 3D graph is unbalanced since the maximum number of different colors (i.e.,  $k_1$ ) is determined by the most dense sphere in a single round. On the other hand, the optimal solution would require multiple iterations of the used coloring algorithm (e.g.,*

---

**Algorithm 1** Greedy-Coloring based Frequency Allocation
 

---

**Require:** The radius  $R$  of a 3D space, the number of aBSs  $N$ , and the threshold of data rate  $\mathcal{R}_{th}$ .

- 1: Construct the Delaunay tetrahedralization;
  - 2: Calculate the optimal spherical radius,  $\epsilon^*$ , as per (39);
  - 3: Fill the space with spheres of radius  $\epsilon^*$  by using FCC packing;
  - 4: For each sphere, count the number of its standard cells and residual cells;
  - 5: Sort the spheres in a descending order by starting with the one having the largest number of cells (say,  $k_1$ ), and define  $W = \{k_1, k_2, \dots, k_n\}$ , where  $k_1 \geq k_2 \geq \dots \geq k_n$ , where  $n$  denotes the number of spheres;
  - 6: **for**  $i := 1$  to  $n$  **do**
  - 7:   **if** Sphere- $i$  has partially colored tetrahedral cells **then**
  - 8:     Assign the smallest number of possible colors to the remaining tetrahedral cells;
  - 9:   **end if**
  - 10: **end for**
  - 11: Identify independent cells;
  - 12: Randomly assign colors (chosen from Sphere-1) to independent cells.
- 

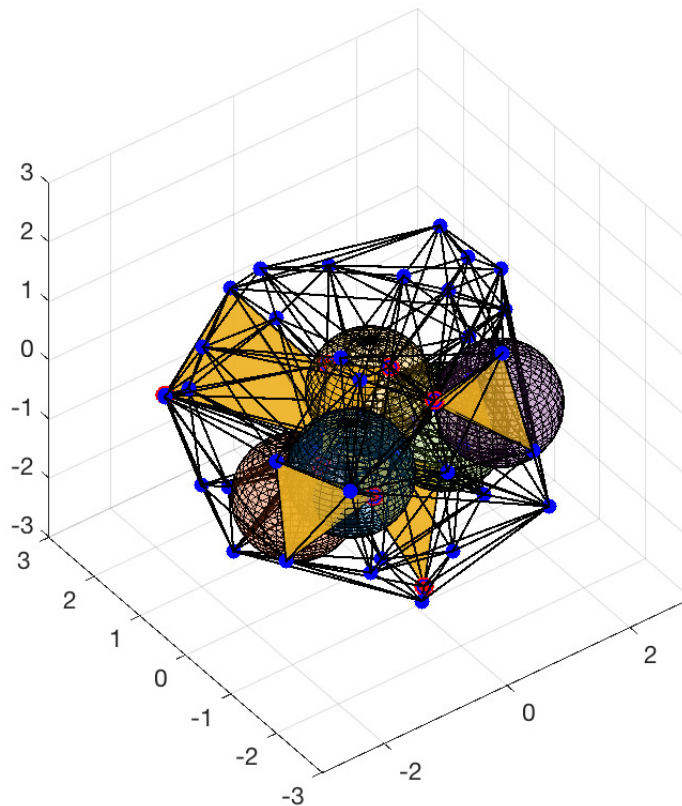


Fig. 7. An illustrative example of frequency allocation.

*balanced coloring [43]) to determine a potentially smaller number of colors. Nevertheless, the latter gain in terms of spectrum resources could be obtained via a considerably higher computational complexity.*

**Remark 2** (The mobility of aUEs). *The considered aBSs typically cover a large coverage area in the introduced aerial platform. Although aBSs are in principle mobile nodes, their mobility is relatively low (since they actually form a backbone aerial network) in comparison to aUEs. Thereby, the frequency allocation/re-allocation process presented herein is reasonably assumed to be static over many communication time-frames, whereas it may alter after significant movement of aBSs. It is also stated that since small-scale channel fading is not present in our approach, the rather costly signaling overhead for instantaneous channel-state information (CSI) acquisition is not required.*

#### D. Interference Analysis

When frequency reuse is implemented amongst the available tetrahedral cells, the interfering aBSs, not all aBSs in  $\Phi$ , which transmit in the same frequency band, are a thinned version of the original BPP with a total number of aBSs  $N' \triangleq (N - 4)/\eta$ . Since a thinned version of a BPP is again a BPP, the ergodic data rate for general aUEs can be computed as

$$\mathcal{R}'_1(\alpha, \eta) = \frac{1}{\eta} \int_{\mathbf{r}>0} \int_{z>0} \frac{1}{z} (1 - M_{S_1}) M'_{I_1}(z, \eta) f_{d_1, d_2, d_3, d_4}(r_1, r_2, r_3, r_4) dz d\mathbf{r}, \quad (42)$$

where  $\mathbf{r} = (r_1, r_2, r_3, r_4)$  with  $r_1 < r_2 < r_3 < r_4$ , and  $M_{S_1}(z)$  is given in (13), and

$$M'_{I_1}(z, \eta) = \left( \frac{1}{R^3 - d_4^3} \int_{d_4}^R 3x^2 \exp(-zx^{-\alpha}) dx \right)^{\frac{N-4}{\eta}} \quad (43)$$

$$= \left( \frac{1}{R^3 - d_4^3} \left( R^3 {}_1F_1 \left[ \begin{matrix} -\frac{3}{\alpha} \\ 1 - \frac{3}{\alpha} \end{matrix}; -zR^{-\alpha} \right] - d_4^3 {}_1F_1 \left[ \begin{matrix} -\frac{3}{\alpha} \\ 1 - \frac{3}{\alpha} \end{matrix}; -zd_4^{-\alpha} \right] \right) \right)^{\frac{N-4}{\eta}}. \quad (44)$$

The same analogy holds also for the worst-case scenario.

Apart from the above thinning BPP, the arising point process (regarding the inter-cluster interference) is sufficiently modeled by a Matérn hard-core point process (MHCPP) of Type I [44]; whereby, there are no points inside  $b(o, \epsilon^*)$ , while they are uniformly placed elsewhere. Given a parent PPP with intensity  $\lambda$ , Type I MHCPP has a corresponding intensity  $\lambda' \triangleq \lambda \exp(-\lambda 4\pi(\epsilon^*)^3/3)$  [22, Section 3.5]. To evaluate the interfering power at the cluster-based system model, the approximation in [45] is adopted where the Type I MHCPP is approximated as a PPP, which follows the conditional intensity  $\lambda'$ . Doing so, referring back to our model with a given number of aBSs  $N$  and with the help of [22, Thm. 2.9 and Def. 2.12], the inter-cluster interference is modeled by a BPP with parameter

$$\psi \triangleq \left[ (N - 4) \exp \left( -(N - 4) \frac{\epsilon^{*3}}{R^3} \right) \right], \quad (45)$$

where  $\lfloor \cdot \rfloor$  is a rounding operator to the closest integer. Then the equivalent frequency reuse factor is

$$\eta' = \left\lfloor \frac{N - 4}{\psi} \right\rfloor. \quad (46)$$

Consequently, each cell can only use  $1/\eta'^{\text{th}}$  of the available frequencies. By substituting  $(N - 4)$  with  $\psi$  in (14), the said conditional interference can approximately be computed with respect to the general user case, expressed as

$$\mathcal{R}'_1(\alpha, \eta') = \frac{1}{\eta'} \int_{r>0} \int_{z>0} \frac{1}{z} (1 - M_{S_1}) M'_{I_1}(z, \eta') f_{d_1, d_2, d_3, d_4}(r_1, r_2, r_3, r_4) dz d\mathbf{r}, \quad (47)$$

where  $M_{S_1}(z)$  and  $M'_{I_1}(\cdot)$  are given by (13) and (44), respectively.

## V. SIMULATION RESULTS AND DISCUSSION

In this section, numerical results computed as per the previously obtained analytical expressions are illustrated, in comparison with extensive Monte-Carlo simulation results. In the pertaining simulation experiments, a large wireless network with coverage volume of  $R = 3$  km is assumed. Since we focus on LoS signal propagation conditions in free-space, the value of path-loss exponent is set to  $\alpha \leq 3.2$ .<sup>3</sup>

### A. Ergodic Data Rate and Coverage Probability

1) *General aUEs*: Figure 8 depicts the ergodic data rate versus the path-loss exponent  $\alpha$  for general aUEs, where the number of aBSs is set to  $N = 50$  or  $N = 150$ . As observed, for a fixed  $N$ , the data rate monotonically increases with  $\alpha$ . It implies that the interfering power decreases more intense compared to the signal power, as  $\alpha$  increases; thereby, improving the ergodic data rate. On the other hand, for a fixed  $\alpha$ , the ergodic data rate decreases for a larger number of aBSs, as interference gets stronger with regards to an increased number of interfering aBSs. For either case, the numerical results computed as per Theorem 1 agree well with the simulation ones, which corroborates the effectiveness of our analysis.

Figure 9 shows the ergodic data rate versus different number of aBSs,  $N$ , for a given threshold data rate  $\mathcal{R}_{\text{th}} = \ln(1 + 10^3) \approx 6.9$  nats/sec/Hz. The corresponding frequency reuse factor is calculated via (41) for the random interference model and (46) for the Type I MHCPP interference model. In fact, the average data rate decreases with an increased density of aBSs, since the frequency reuse factor is increasing as the number of aBSs also increases for a fixed rate threshold, while the data rate decreases with an increased

<sup>3</sup>Although the path-loss exponent  $\alpha$  is practically assumed to be much less than 3, it can also be applicable for the scenario with  $\alpha$  being greater than 3. Note that the path-loss exponent  $\alpha$  is environment-related and can be approximately ranged from 1.6 (e.g., hallways inside buildings) to 8 (e.g., dense urban environments) [46, p. 41], with  $\alpha = 2$  corresponding to free-space signal propagation.

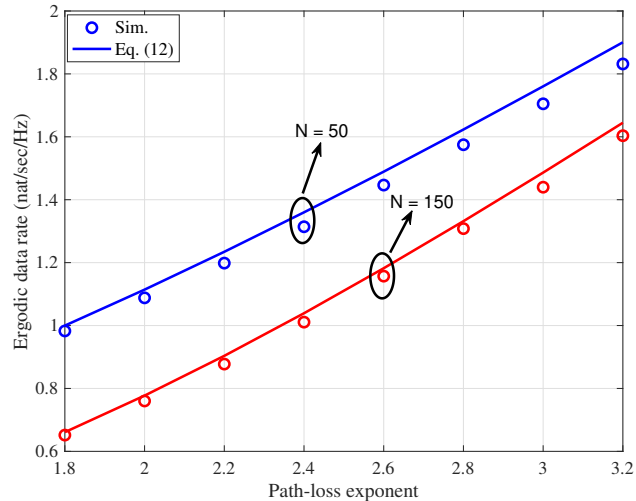


Fig. 8. Ergodic data rate of general aUEs versus the path-loss exponent  $\alpha$  with  $N = 50$  and  $N = 150$ .

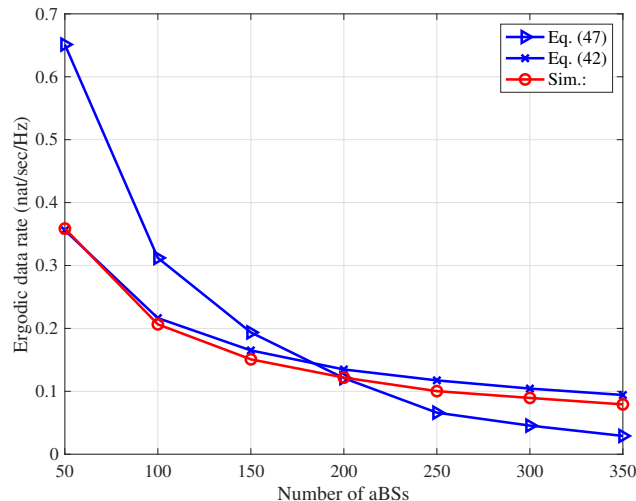


Fig. 9. Ergodic data rate of general aUEs versus the number of aBSs  $N$  with  $\alpha = 2$  and  $\mathcal{R}_{\text{th}} = \ln(1 + 10^3) \approx 6.9$  nats/sec/Hz.

reuse factor. On the other hand, it can be seen that the numerical results of (42) based on a thinning BPP are sharply close to the simulated ones, compared to the ones based on (47). This is consistent to our approach, adopting the tractable randomized frequency assignment scheme. It is also revealed that the correlation between points in a Type I MHCPP make the properties of a BPP no longer valid.

Figure 10 illustrates the coverage probability versus the SIR threshold, with different path-loss exponent  $\alpha$ . It can be observed that the coverage probability increases with  $\alpha$ , since larger  $\alpha$  implies lower interference. Besides, the numerical results computed as per Theorem 2 also match well with the corresponding simulated ones, which further verifies the accuracy of the proposed approach.

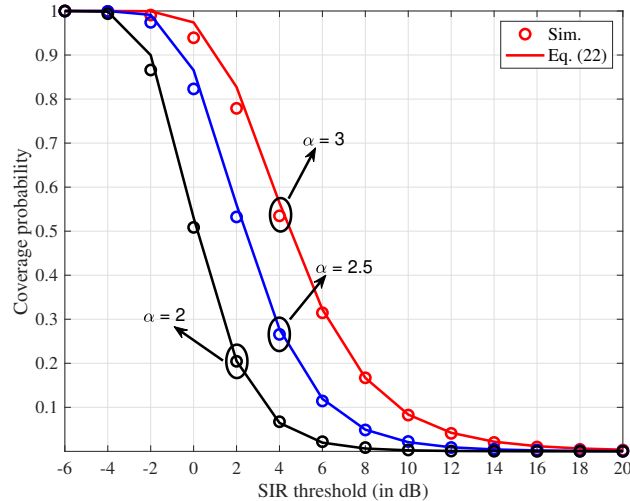


Fig. 10. Coverage probability of general aUEs versus the SIR threshold in the unit of dB, with  $N = 150$ .

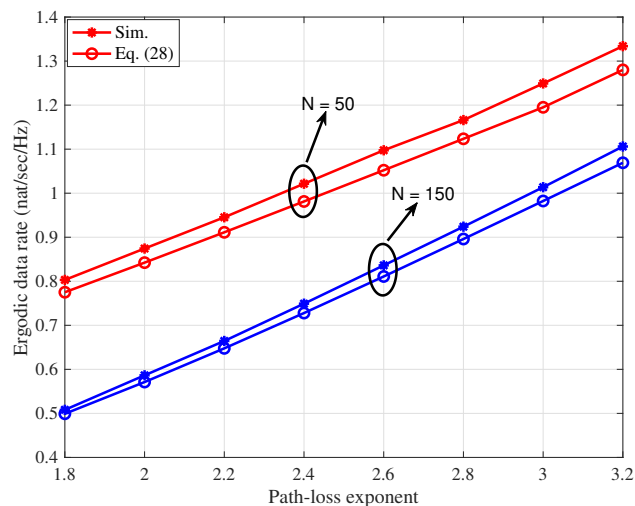


Fig. 11. Ergodic data rate of the worst-case aUEs versus the path-loss exponent  $\alpha$  with  $N = 50$  and  $N = 150$ .

2) *Worst-case aUEs*: Figure 11 shows the ergodic data rate versus the path-loss exponent  $\alpha$  for the worst-case aUEs. It is noted that the analytical results lower bound the simulation ones. In fact, this underestimation is introduced by the assumption of independence between aBSs and a typical aUE. More specifically, by recalling the Slivnyak-Mecke theorem in stochastic geometry [36, p. 132], a typical aUE is assumed to be located at the origin  $(0, 0, 0) \in \mathbb{R}^3$ , without loss of generality. This assumption implies that the location of a typical aUE is independent of aBSs' location. However, as far as the worst-case aUE is concerned, a typical aUE maintains the same distance from its four nearest aBSs. Obviously, the location of a typical aUE here directly depends on the locations of its closest aBSs. Such a dependence results in an

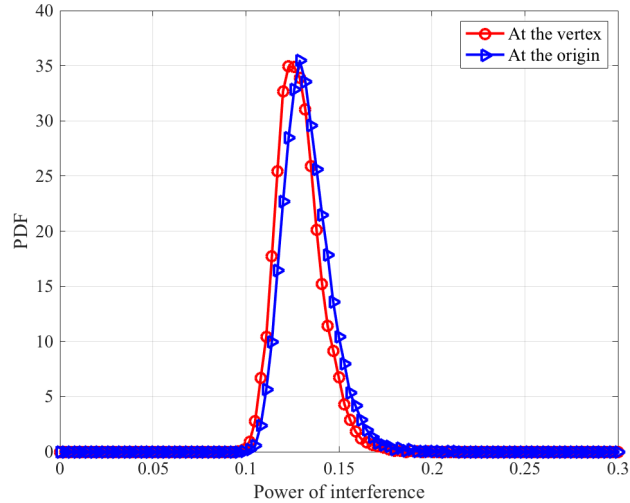


Fig. 12. PDFs of the interference at the origin and at the vertex.

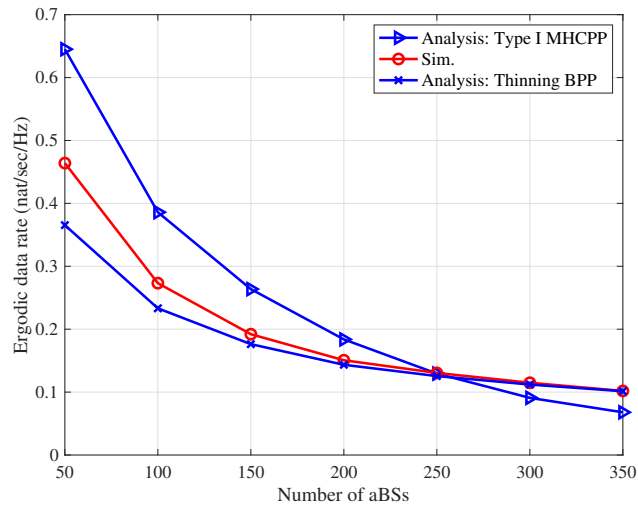


Fig. 13. Ergodic data rate of the worst-case aUEs versus the number of aBSs  $N$  with  $\alpha = 2$  and  $\mathcal{R}_{\text{th}} = \ln(1 + 10^3) \approx 6.9$  nats/sec/Hz.

overestimation of the total interfering power as further shown in Fig. 12. The same observation is found in Fig. 13, where the analytical results are a little bit lower than the simulation ones. It is significantly noted that, although ergodic data rate is decreasing with the number of aBSs, the simulated ergodic data rate of the worst-case aUEs is higher than that of general aUEs as shown in Fig. 9, which acts as a performance upper bound. The same observation is also reflected in Fig. 14, where the analytical results slightly deviate (i.e., overestimate the total interfering power) from the corresponding simulated ones. It is noteworthy that, although the interfering power is approximated by the Gamma distribution, the said deviation caused by the interference approximation given in (19) is rather marginal (the analytical coverage probability is

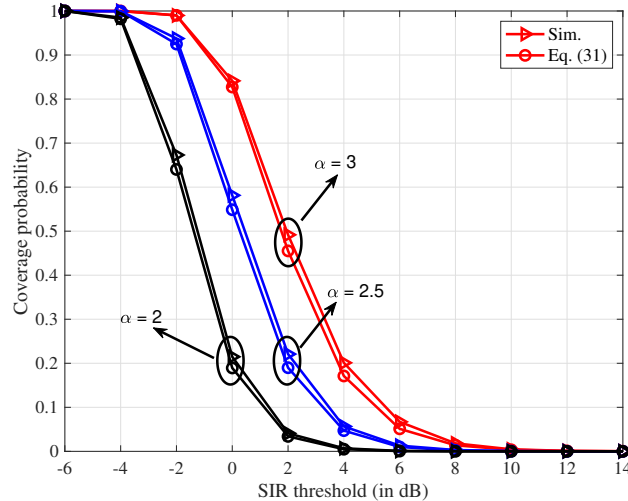


Fig. 14. Coverage probabilities of the worst-case aUEs versus the SIR threshold in the unit of dB with  $N = 150$ .

well matched with the simulation results for the general aUE case as shown in Fig. 10). The reason for such a mismatch comes indeed from the independent assumption of the typical aUE.

### B. Binomial-Delaunay Tetrahedralization vs. Binomial-Voronoi Tessellation

1) *Comparison with binomial-Voronoi tessellation without CoMP*: Figure 15 illustrates the coverage probability of general aUEs versus the SIR threshold, where the path-loss exponent was set to  $\alpha = 2$  or  $\alpha = 3$ . It is observed that the coverage probability in our proposed model is much higher than that in the scheme without CoMP, even at a (relatively) high value of  $\alpha = 3$ . This emphatically manifests that cooperative communication is quite necessary, especially in the presence of ICI.

2) *Comparison with binomial-Voronoi tessellation with dynamic cooperation set*: For binomial-Voronoi tessellation utilizing a dynamic cooperation set, the typical aUE is always located at the center of its serving aBSs, belonging to a aUE-centric scheme. In this scheme, the typical aUE exhaustively searches every aBS so as to determine the appropriate aBS whereby it receives the strongest signals. Then, aUE can choose one, two, or more aBSs to cooperate and enhance its received SINR, at the cost of searching complexity and feedback (signaling) overhead. It turns out that the resultant aBS set does not always include the four nearest aBSs. This scheme is fundamentally different from our proposed approach, which is aBS-centric (i.e., all aUEs within a cell are being served by an identical fixed and location-dependent aBS set). For the worst-case aUE, the serving aBSs are the four nearest aBSs with equal distance. On this condition, the signal power in the aUE-centric case is equivalent to that of an aBS-centric case; the same outcome also



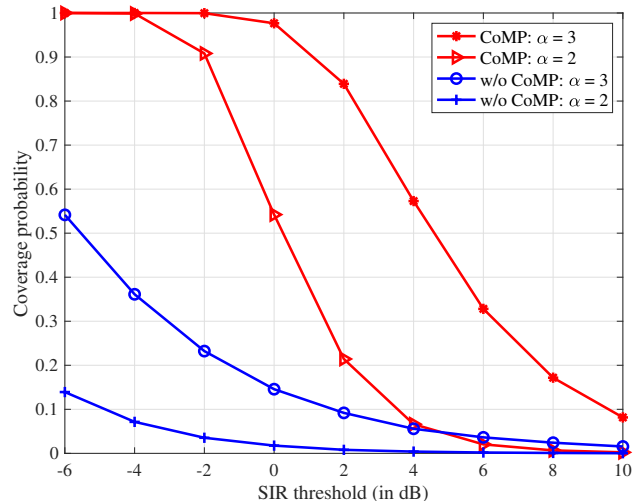


Fig. 15. Coverage probabilities of general aUEs versus the SIR threshold in the unit of dB under the proposed Delaunay CoMP scheme and binomial-Voronoi tessellation scheme without CoMP and  $N = 150$ .

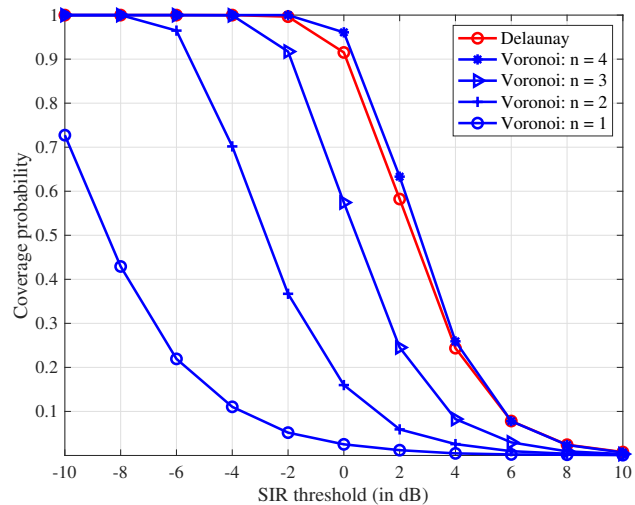


Fig. 16. Coverage probabilities for a typical aUE simulated under the proposed Delaunay CoMP scheme and binomial-Voronoi tessellation scheme with  $n = \{1, 2, 3, 4\}$  dynamic cooperating BSs and  $N = 50$ .

holds for the interfering power. For the general aUE case, without loss of generality, we choose the origin as the typical aUE. The simulation results are presented in Fig. 16. It can be seen that the performance under the two schemes is comparable, which further implies that the serving aBSs at the vertices of a tetrahedral cell in our approach can be well approximated as the nearest four ones. Most importantly, it is verified that the proposed approach presents quite a similar performance as the conventional approach; yet, introducing considerably reduced computational efforts and feedback overhead.

## VI. CONCLUSION

In this paper, a novel 3D cellular model was proposed. CoMP was adopted to enhance the communication quality, based on binomial-Delaunay tetrahedralization; whereby, each aUE in a tetrahedral cell can be jointly served by its four nearest aBSs, thus providing reliable and high throughput connectivity. Analytical formulae regarding the ergodic capacity and coverage probability were offered for two user cases, namely, general aUE and worst-case aUE. It turns out that CoMP brings significant performance gain to the considered system setup in the presence of ICI. Also, a fair comparison with the classical binomial-Voronoi approach with a dynamic cooperation set was also conducted. Simulation and numerical results explicitly indicated that our proposed approach is comparable to the dynamic scheme, yet introducing much less computational burden and signaling overhead. Finally, a practical frequency allocation scheme based on a fast greedy coloring algorithm was analytically presented, which provides a benchmark for future network planning in 3D aerial networking infrastructures.

### APPENDIX A

#### DERIVATION OF EQ. (9)

The joint density function of the ordered distance  $d_i, i = 5 : N$  conditioned on the serving distance  $d_4$  is given by

$$f_{d_5, d_6, \dots, d_N | d_4}(r_5, r_6, \dots, r_N) = \frac{f_{d_4, d_5, \dots, d_N}(r_4, r_5, \dots, r_N)}{f_{d_4}(r_4)}, \quad (\text{A.1})$$

where the joint distribution of the numerator can be computed as

$$\begin{aligned} f_{d_4, d_5, \dots, d_N}(r_4, r_5, \dots, r_N) &= \int_{r_1 > 0} \int_{r_2 > r_1} \int_{r_3 > r_2} f_{d_1, d_2, \dots, d_N}(r_1, r_2, \dots, r_N) dr_3 dr_2 dr_1 \\ &= \int_{r_1 > 0} \int_{r_2 > r_1} \int_{r_3 > r_2} N! \prod_{i=1}^N f_{D_i}(r_i) dr_3 dr_2 dr_1 \end{aligned} \quad (\text{A.2})$$

$$\begin{aligned} &= N! \prod_{i=4}^N f_{D_i}(r_i) \int_{r_1 > 0} \int_{r_2 > r_1} \int_{r_3 > r_2} \prod_{i=1}^3 f_{D_i}(r_i) dr_3 dr_2 dr_1 \\ &= N! \prod_{i=4}^N f_{D_i}(r_i) \frac{1}{3!} \prod_{i=1}^3 \int_0^{r_3} f_{D_i}(r_i) dr_i \end{aligned} \quad (\text{A.3})$$

$$= \frac{N!}{3!} \prod_{i=4}^N f_{D_i}(r_i) [F_D(r_3)]^3, \quad (\text{A.4})$$

where (A.2) follows from the definition of the joint distance distribution based on the equality in [47, Eq. (2.10)], (A.3) follows from the symmetry of [47, Eq. (2.12)]. According to [23, Eq. (4)], the fourth

nearest distance distribution can be rewritten as

$$f_{d_4}(r_4) = \frac{N!}{3!(N-4)!} [F_D(r_4)]^3 [1 - F_D(r_4)]^{N-4} f_D(r_4). \quad (\text{A.5})$$

Inserting (A.4) and (A.5) into (A.1) yields

$$f_{d_5, d_6, \dots, d_N | d_4}(r_5, r_6, \dots, r_N) = (N-4)! \prod_{i=5}^N \frac{f_D(r_i)}{1 - F_D(r_4)}. \quad (\text{A.6})$$

Note that there are  $(N-4)!$  number of possible permutations of the ordered distances  $d_i, i = 5, 6, \dots, N$ . Since the interfering aBSs are chosen uniformly at random, the permutation term does not appear in the conditional joint distribution of the unordered distances set [27, Appendix A], that is

$$f_{d_5, d_6, \dots, d_N | d_4}(r_5, r_6, \dots, r_N) = \prod_{i=5}^N \frac{f_D(r_i)}{1 - F_D(r_4)}, \quad (\text{A.7})$$

then, the sampling distribution of the  $N-4$  i.i.d. random variables is given by

$$f_{D_i | r}(r_i) = \frac{f_D(r_i)}{1 - F_D(r_4)}, \quad (\text{A.8})$$

where  $f_D(r_i)$  is shown in (8). Finally, substituting (7) and (8) into (A.8) yields (9).

## APPENDIX B PROOF OF LEMMA 1

By recalling the causal form of the central limit theorem [40, p. 234], it is known that the distribution of the sum  $I_1 \triangleq \sum_{k=5}^N d_{k,0}^{-\alpha}$  can be approximated by the Gamma distribution given by (19), with the parameters determined by

$$v(d) = \frac{\mathbb{E}^2(I_1)}{\text{Var}(I_1)} \quad (\text{B.1})$$

and

$$\theta(d) = \frac{\text{Var}(I_1)}{\mathbb{E}(I_1)}, \quad (\text{B.2})$$

where the operators  $\mathbb{E}(I_1)$  and  $\text{Var}(I_1)$  denote the mean value and variance of  $I_1$ , respectively.

By virtue of (9), the mean interference power conditioned on the serving distance  $d_4$  is computed as

$$\mathbb{E}(I_1) = (N-4) \int_d^R x^{-\alpha} \frac{3x^2}{R^3 - d^3} dx = \begin{cases} 3(N-4) \frac{1}{3-\alpha} \frac{1}{R^3 - d^3} (R^{3-\alpha} - d^{3-\alpha}), & \alpha \neq 3, \\ 3(N-4) \frac{1}{R^3 - d^3} (\ln R - \ln d), & \alpha = 3. \end{cases} \quad (\text{B.3})$$

Likewise, the conditional variance of interference power can be derived as

$$\text{Var}(I_1) = (N - 4) \left[ \int_d^R x^{-2\alpha} \frac{3x^2}{R^3 - d^3} dx - \left( \int_d^R x^{-\alpha} \frac{3x^2}{R^3 - d^3} dx \right)^2 \right] \quad (\text{B.4})$$

$$= \begin{cases} (N - 4) \left[ \frac{3}{3-2\alpha} \frac{1}{R^3-d^3} (R^{3-2\alpha} - d^{3-2\alpha}) - \frac{9}{(3-\alpha)^2} \frac{(R^{3-2\alpha}-d^{3-2\alpha})^2}{(R^3-d^3)^2} \right], & \alpha \neq 3, \\ (N - 4) \left[ \frac{1}{R^3-d^3} (d^{-3} - R^{-3}) - \left[ \frac{3}{R^3-d^3} (\ln R - \ln d) \right]^2 \right], & \alpha = 3. \end{cases} \quad (\text{B.5})$$

Finally, in light of (B.1), (B.2), (B.3) and (B.4) and after performing some algebraic manipulations, we attain (20) and (21), which completes the proof.

### APPENDIX C

#### DERIVATION OF EQ. (27)

Let a new process be defined as  $\Phi(W) = N$ , i.e., a process having exactly  $N$  points uniformly distributed in  $W$ . The resulting set is a binomial point process, which is in fact a conditional PPP  $\Phi$  with  $\Phi(W) = N$  [36, p. 43]. Let  $b(o, r)$  be a 3D ball of radius  $r$  centered at  $o$ . The probability that there are  $k$  points in  $b(o, r)$  is given by [48, Eq. (13)], which reads

$$\Pr[\Phi[b(o, r)] = k | \Phi(W) = N] = \binom{N}{k} p^k (1-p)^{N-k}, \quad 0 \leq r \leq R, \quad (\text{C.1})$$

where  $p = \frac{V[b(o, r) \cap W]}{V[W]} = \left(\frac{r}{R}\right)^3$ , and  $V[b(o, r) \cap W]$  and  $V[W]$  are the volume of  $b(o, r) \cap W$  and  $W$ , respectively.

Assume the distance between the vertex and its nearest  $k$  neighbors is denoted by  $d$ ; then, the corresponding distribution function  $F_d(\delta)$  is calculated as

$$F_d(\delta) = \lim_{\epsilon \rightarrow 0} \frac{\int_0^\delta \Pr[\Phi(b(o, x)) = 0, \Phi(b(o, x + \epsilon) \setminus b(o, x)) = k | \Phi(W) = N] dx}{\int_0^R \Pr[\Phi(b(o, x)) = 0, \Phi(b(o, x + \epsilon) \setminus b(o, x)) = k, \Phi(W) = N] dx}. \quad (\text{C.2})$$

Using a similar simplification technique as in [49, Section 6], we arrive at

$$\begin{aligned} F_d(\delta) &= \lim_{\epsilon \rightarrow 0} \frac{\int_0^\delta \binom{N}{k} \left[ \frac{1}{R^3} ((x + \epsilon)^3 - x^3) \right]^k \left[ 1 - \left(\frac{x}{R}\right)^3 \right]^{N-k} dx}{\int_0^R \binom{N}{k} \left[ \frac{1}{R^3} ((x + \epsilon)^3 - x^3) \right]^k \left[ 1 - \left(\frac{x}{R}\right)^3 \right]^{N-k} dx} \\ &= \frac{\int_0^\delta x^{(3-1)k} \left[ 1 - \left(\frac{x}{R}\right)^3 \right]^{N-k} dx}{\int_0^R x^{(3-1)k} \left[ 1 - \left(\frac{x}{R}\right)^3 \right]^{N-k} dx}. \end{aligned} \quad (\text{C.3})$$

Differentiating and using [38, Eq. (8.380.1)], it yields

$$f_a(\delta) = \frac{3}{R\beta\left(N-k, \left(1-\frac{1}{3}\right)^k + \frac{1}{3}\right)} \left(\frac{\delta}{R}\right)^{(3-1)k} \left[1 - \left(\frac{\delta}{R}\right)^3\right]^{N-k}, \quad (\text{C.4})$$

where  $\beta(x, y) \triangleq \int_0^1 t^{x-1}(1-t)^{y-1}dt$  is the Beta function. Finally, substituting  $k = 4$  into (C.4) yields the desired (27).

## REFERENCES

- [1] M. Mozaffari, W. Saad, M. Bennis, Y. Nam, and M. Debbah, "A tutorial on UAVs for wireless networks: Applications, challenges, and open problems," *IEEE Commun. Surveys Tuts.*, vol. 21, no. 3, pp. 2334–2360, Thirdquarter 2019.
- [2] S. Hayat, E. Yanmaz, and R. Muzaffar, "Survey on unmanned aerial vehicle networks for civil applications: A communications viewpoint," *IEEE Commun. Surveys Tuts.*, vol. 18, no. 4, pp. 2624–2661, Fourthquarter 2016.
- [3] W. Saad, M. Bennis, and M. Chen, "A vision of 6G wireless systems: Applications, trends, technologies, and open research problems," *IEEE Netw.*, to appear, 2020. [Online]. Available: <https://ieeexplore.ieee.org/document/8869705/>
- [4] M. M. Azari, F. Rosas, A. Chiumento, and S. Pollin, "Coexistence of terrestrial and aerial users in cellular networks," in *2017 IEEE Glob. Workshops (GC Wkshps)*, Dec. 2017, pp. 1–6.
- [5] G. Geraci, A. Garcia-Rodriguez, L. G. Giordano, D. Lopez-Perez, and E. Björnson, "Supporting UAV cellular communications through massive MIMO," in *2018 IEEE Int. Conf. Commun. Workshops (ICC Workshops)*, May 2018, pp. 1–6.
- [6] X. Yu, J. Zhang, R. Schober, and K. B. Letaief, "A tractable framework for coverage analysis of cellular-connected UAV networks," in *2019 IEEE Int. Conf. Commun. Workshops (ICC Workshops)*, May 2019, pp. 1–6.
- [7] M. M. Azari, F. Rosas, and S. Pollin, "Cellular connectivity for UAVs: Network modeling, performance analysis, and design guidelines," *IEEE Trans. Wireless Commun.*, vol. 18, no. 7, pp. 3366–3381, July 2019.
- [8] F. Cui, Y. Cai, Z. Qin, M. Zhao, and G. Y. Li, "Multiple access for mobile-UAV enabled networks: Joint trajectory design and resource allocation," *IEEE Trans. Commun.*, vol. 67, no. 7, pp. 4980–4994, July 2019.
- [9] M. Mozaffari, W. Saad, M. Bennis, and M. Debbah, "Wireless communication using unmanned aerial vehicles (UAVs): Optimal transport theory for hover time optimization," *IEEE Trans. Wireless Commun.*, vol. 16, no. 12, pp. 8052–8066, Dec. 2017.
- [10] M. Alzenad, A. El-Keyi, F. Lagum, and H. Yanikomeroglu, "3-D placement of an unmanned aerial vehicle base station (UAV-BS) for energy-efficient maximal coverage," *IEEE Wireless Commun. Lett.*, vol. 6, no. 4, pp. 434–437, Aug. 2017.
- [11] V. V. Chetlur and H. S. Dhillon, "Downlink coverage analysis for a finite 3-D wireless network of unmanned aerial vehicles," *IEEE Trans. Commun.*, vol. 65, no. 10, pp. 4543–4558, Oct. 2017.
- [12] H. Wu, X. Tao, N. Zhang, and X. Shen, "Cooperative UAV cluster-assisted terrestrial cellular networks for ubiquitous coverage," *IEEE J. Select. Areas Commun.*, vol. 36, no. 9, pp. 2045–2058, Sep. 2018.
- [13] Y. Zhu, G. Zheng, and M. Fitch, "Secrecy rate analysis of UAV-enabled mmwave networks using Matérn hardcore point processes," *IEEE J. Select. Areas Commun.*, vol. 36, no. 7, pp. 1397–1409, July 2018.
- [14] P. K. Sharma and D. I. Kim, "Random 3D mobile UAV networks: Mobility modeling and coverage probability," *IEEE Trans. Wireless Commun.*, vol. 18, no. 5, pp. 2527–2538, May 2019.
- [15] M. Mozaffari, A. T. Z. Kasgari, W. Saad, M. Bennis, and M. Debbah, "Beyond 5G with UAVs: Foundations of a 3D wireless cellular network," *IEEE Trans. Wireless Commun.*, vol. 18, no. 1, pp. 357–372, Jan. 2019.
- [16] J. Ye, C. Zhang, H. Lei, G. Pan, and Z. Ding, "Secure UAV-to-UAV systems with spatially random UAVs," *IEEE Wireless Commun. Lett.*, vol. 8, no. 2, pp. 564–567, Apr. 2019.
- [17] S. Zhang, H. Zhang, B. Di, and L. Song, "Cellular UAV-to-X communications: Design and optimization for multi-UAV networks," *IEEE Trans. Wireless Commun.*, vol. 18, no. 2, pp. 1346–1359, Feb. 2019.
- [18] G. Nigam, P. Minero, and M. Haenggi, "Coordinated multipoint joint transmission in heterogeneous networks," *IEEE Trans. Commun.*, vol. 62, no. 11, pp. 4134–4146, Nov. 2014.
- [19] J. G. Andrews, F. Baccelli, and R. K. Ganti, "A tractable approach to coverage and rate in cellular networks," *IEEE Trans. Commun.*, vol. 59, no. 11, pp. 3122–3134, Nov. 2011.

- [20] S. Y. Jung, H. K. Lee, and S. L. Kim, "Worst-case user analysis in Poisson Voronoi cells," *IEEE Commun. Lett.*, vol. 17, no. 8, pp. 1580–1583, Aug. 2013.
- [21] X. Yu, Q. Cui, and M. Haenggi, "Coherent joint transmission in downlink heterogeneous cellular networks," *IEEE Wireless Commun. Lett.*, vol. 7, no. 2, pp. 274–277, Apr. 2018.
- [22] M. Haenggi, *Stochastic Geometry for Wireless Networks*. Cambridge University Press, 2012.
- [23] S. Srinivasa and M. Haenggi, "Distance distributions in finite uniformly random networks: Theory and applications," *IEEE Trans. Veh. Technol.*, vol. 59, no. 2, pp. 940–949, Feb. 2010.
- [24] J. Guo, S. Durrani, and X. Zhou, "Outage probability in arbitrarily-shaped finite wireless networks," *IEEE Trans. Commun.*, vol. 62, no. 2, pp. 699–712, Feb. 2014.
- [25] D. Torrieri and M. C. Valenti, "The outage probability of a finite ad hoc network in Nakagami fading," *IEEE Trans. Commun.*, vol. 60, no. 11, pp. 3509–3518, Nov. 2012.
- [26] J. Chen, M. Ding, and Q. T. Zhang, "Interference statistics and performance analysis of MIMO ad hoc networks in binomial fields," *IEEE Trans. Veh. Technol.*, vol. 61, no. 5, pp. 2033–2043, June 2012.
- [27] M. Afshang and H. S. Dhillon, "Fundamentals of modeling finite wireless networks using binomial point process," *IEEE Trans. Wireless Commun.*, vol. 16, no. 5, pp. 3355–3370, May 2017.
- [28] Z. Khalid and S. Durrani, "Distance distributions in regular polygons," *IEEE Trans. Veh. Technol.*, vol. 62, no. 5, pp. 2363–2368, June 2013.
- [29] M. Xia and S. Aïssa, "Unified analytical volume distribution of Poisson-Delaunay simplex and its application to coordinated multi-point transmission," *IEEE Trans. Wireless Commun.*, vol. 17, no. 7, pp. 4912–4921, July 2018.
- [30] Y. Li, M. Xia, and S. Aïssa, "Coordinated multi-point transmission: A Poisson-Delaunay triangulation based approach," *IEEE Trans. Wireless Commun.*, to appear, 2020. [Online]. Available: <https://ieeexplore.ieee.org/document/8976426>
- [31] J. Liu, Y. Shi, Z. M. Fadlullah, and N. Kato, "Space-air-ground integrated network: A survey," *IEEE Commun. Surveys Tuts.*, vol. 20, no. 4, pp. 2714–2741, Fourthquarter 2018.
- [32] V. T. Rajan, "Optimality of the Delaunay triangulation in  $\mathbb{R}^d$ ," *Discrete Comput. Geometry*, vol. 12, no. 2, pp. 189–202, 1994.
- [33] A. Okabe, B. Boots, K. Sugihara, and S. N. Chiu, *Spatial Tessellations: Concepts and Applications of Voronoi Diagrams*. 2nd ed. New York, NY, USA: Wiley, 2000.
- [34] J. H. Conway and N. J. A. Sloane, *Sphere Packings, Lattices, and Groups*, 3rd ed. Springer, 1999.
- [35] A. L. Hinde and R. E. Miles, "Monte Carlo estimates of the distributions of the random polygons of the Voronoi tessellation with respect to a Poisson process," *J. Statist. Comput. Simul.*, vol. 10, no. 3-4, pp. 205–223, 1980.
- [36] S. N. Chiu, D. Stoyan, W. S. Kendall, and J. Mecke, *Stochastic Geometry and Its Applications*, 3rd ed. John Wiley & Sons, 2013.
- [37] H. A. David and H. N. Nagaraja, *Order Statistics*, 3rd ed. John Wiley & Sons, 2003.
- [38] I. S. Gradshteyn and I. M. Ryzhik, *Table of Integrals, Series and Products*, 6th ed. Academic Press, 2000.
- [39] K. A. Hamdi, "A useful lemma for capacity analysis of fading interference channels," *IEEE Trans. Commun.*, vol. 58, no. 2, pp. 411–416, Feb. 2010.
- [40] A. Papoulis, *The Fourier Integral and Its Applications*. McGraw-Hill Book Company, Inc., 1962.
- [41] T. C. Hales, "A proof of the Kepler conjecture," *Annals of Mathematics*, vol. 162, pp. 1065–1185, 2005.
- [42] Ø. Hjelle and M. Dæhlen, *Triangulations and Applications*. Springer, 2006.
- [43] A. Kosowski and K. Manuszewski, "Classical coloring of graphs," *Contemp. Math.*, vol. 352, pp. 1–20, June 2004.
- [44] B. Matérn, "Spatial variation," in *Meddelanden Fran Statens Skogsforskningsinstitut*, vol. 49, no. 5, 1960.
- [45] M. Haenggi, "Mean interference in hard-core wireless networks," *IEEE Commun. Lett.*, vol. 15, no. 8, pp. 792–794, Aug. 2011.
- [46] A. Goldsmith, *Wireless Communication*. Cambridge University Press, 2005.
- [47] M. Ahsanullah and V. B. Nevzorov, *Order Statistics: Examples and Exercises*. New York, USA: Nova Science Publishers, 2005.
- [48] D. Moltchanov, "Distance distributions in random networks," *Ad Hoc Netw.*, vol. 10, no. 6, pp. 1146–1166, Mar. 2012.
- [49] L. Muche, "The Poisson-Voronoi tessellation: Relationships for edges," *Advances in Applied Probability*, vol. 37, no. 2, pp. 279–296, Dec. 2004.